Er^{3+} impurities in $KTiOPO_4$ studied by electron paramagnetic resonance

2006 J. Phys.: Condens. Matter 18 6655

(http://iopscience.iop.org/0953-8984/18/29/007)

INSTITUTE OF PHYSICS PUBLISHING JOURNAL OF PHYSICS: CONDENSED MATTER

J. Phys.: Condens. Matter **18** (2006) 6655–6663 doi:10.1088/0953-8984/18/29/007

Er^{3+} impurities in $KTiOPO_4$ studied by electron paramagnetic resonance

D Bravo[1,4], A Martín[2], J J Carvajal[3], M Aguiló[3], F Díaz[3] and F J López[1]

[1] Departamento Física de Materiales, Universidad Autónoma de Madrid, Cantoblanco, 28049 Madrid, Spain
[2] Departamento Física e Instalaciones, ETS Arquitectura, Universidad Politécnica Madrid, Avenida Juan de Herrera 4, 28040 Madrid, Spain
[3] Física i Cristallografia de Materials (FiCMA), Universitat Rovira i Virgili (URV), Campus Sescelades, c/ Marcellí Domingo, s/n, 43007-Tarragona, Spain

E-mail: david.bravo@uam.es

Received 9 February 2006, in final form 23 May 2006
Published 30 June 2006
Online at stacks.iop.org/JPhysCM/18/6655

Abstract

An electron paramagnetic resonance (EPR) study of Er^{3+} ions in single crystals of $KTiOPO_4$ (KTP) is presented. The EPR spectra show the existence of eight different Er^{3+} centres. The g-matrix has been determined for all eight centres from the analysis of the angular dependences of the spectrum in three planes of the crystal. This study provides strong evidence about incorporation of erbium in the low-symmetry K^+ sites of KTP. Possible reasons for the appearance of such a large number of Er^{3+} centres are discussed.

1. Introduction

Potassium titanyl phosphate ($KTiOPO_4$ or KTP) is a well known optoelectronic material. It presents high nonlinear optical coefficients, high optical damage threshold, and thermally stable phase-matching properties, which make it useful for waveguide devices. Also, it is the most used material for second-harmonic generation of Nd–YAG lasers [1, 2]. KTP crystals containing laser-active impurities, such as rare earth (RE) elements, are good candidates to develop self-doubled solid-state lasers. In addition, Er-doped KTP is particularly attractive for application in optical communication devices due to the photoluminescence emission of Er^{3+} around 1.5 μm, which coincides with the low-loss window of standard optical communication fibres.

In order to optimize the performance of devices based on Er-doped KTP it is very important to know the nature of the active centres involved, i.e., the valence of the impurities, their local symmetry and location in the crystal lattice, as well as the number of centres formed. The electron paramagnetic resonance (EPR) technique has proven to be very useful to obtain

[4] Author to whom any correspondence should be addressed.

such basic information for many materials. In fact, EPR has been already used in KTP to study various centres related to transition-metal-ion elements; namely, Fe^{3+} and Cr^{3+} [3, 4], VO^{2+} [5], V^{4+} [6], Mo^{5+} [7], Rh^{2+} [8], WO^{3+} [9], Pt^{3+} and Pt^{+} [10]. All these transition-metal-ion impurities have been found by EPR to be located at both Ti sites existing in KTP (see section 2), except for Pt^{+} impurities, which have been suggested to be substituting for K [10].

On the other hand, no EPR studies of RE-doped KTP exist in the literature. The spectroscopic properties of this material doped with Nd or Er have been investigated by optical absorption and luminescence [11–13]. In these works it has been proposed that Nd^{3+} [11] and Er^{3+} [12, 13] impurities substitute for Ti. However, no conclusive evidence has been given in the literature about substitution of RE-elements for K or Ti, or simultaneously for both. It must be noted that substitution for P has not been considered, mainly due to the large size mismatch between RE^{3+}-elements and P^{5+} [11, 12].

In the present work we have studied the EPR spectra of Er-doped KTP single crystals. Up to eight different Er^{3+} centres have been identified and their g-matrices have been determined. From this study we give evidence for the location of all Er centres at the K sites.

2. Experimental details

Single crystals of Er-doped KTP studied in this work have been grown by the top-seeded solution growth and slow-cooling method, using K_2CO_3, $NH_4H_2PO_4$, TiO_2 and Er_2O_3 as initial reagents that were mixed in the desired proportion. The experiments were made in a vertical cylindrical furnace controlled by a Eurotherm 818P controller/programmer, using cylindrical platinum crucibles, 50 mm in diameter and 65 mm in height, filled with about 100 g of solution. KTP crystal seeds, fixed 15 mm out of the centre of the solution surface, were used for the nucleation of the crystals. During the growth process the temperature was decreased at an average rate of 2 K/day. After eight days, single crystals with dimensions between 2 and 13 mm, depending on the crystallographic direction, were obtained. The erbium concentration was measured by Rutherford back-scattering and atomic absorption techniques, giving a mean value of 2×10^{18} cm^{-3}. More details on the growth procedure have been reported previously [14]. Prismatic samples, with dimensions $2 \times 2 \times 4$ mm^3, were oriented by using a D5000 Siemens x-ray diffractometer equipped with an open Eulerian cradle, and cut with their faces perpendicular to the crystallographic axes a, b and c. The x-ray diffraction characterization also excluded the presence of any additional crystalline phase, the sample being only constituted by the KTP phase. The samples were mounted on a goniometer for measurements of the angular dependence of the EPR spectra.

EPR spectra were recorded at 5 K using a Bruker ESP 300E X-band spectrometer with field modulation of 100 kHz. The temperature of the sample was controlled with an Oxford ESR 9 He-flux cryostat. Accurate values for the frequency and magnetic field were measured using a microwave-frequency counter (Hewlett-Packard 5342A) and an NMR gaussmeter (Bruker ER 035M), respectively.

The crystal structure of KTP was solved by Tordjman *et al* [15] and later refined by Thomas *et al* [16]. The structure is orthorhombic, with space group $Pna2_1$ and lattice parameters $a = 12.819(3)$ Å, $b = 6.399(1)$ Å and $c = 10.584(2)$ Å [16]. There are two crystallographically distinct sites for each cation in the unit cell (labelled as Ti1, Ti2, K1, K2, P1 and P2) and ten independent oxygen sites (labelled as O1–O8, OT1 and OT2). All those sites have point symmetry C_1. Figure 1 shows a partial scheme of the structure for each cation site and their oxygen ligands. To complete the structure within the unit cell, each ion has to be replicated in four positions by the symmetry operations of the space group (identity, two glide

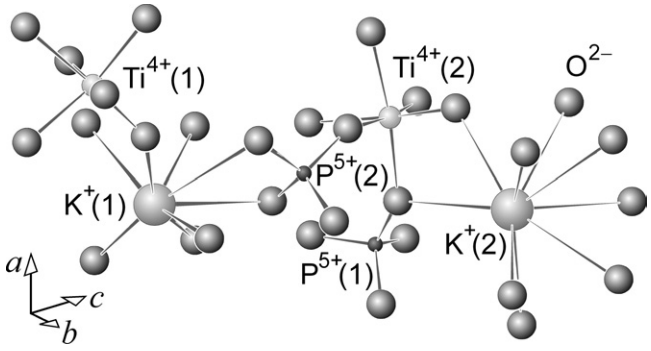

Figure 1. Partial scheme of the KTP structure showing the crystallographic axes a, b and c. Cationic sites K1, K2, Ti1, Ti2, P1 and P2 are shown together with their oxygen ligands (see text for explanation).

Table 1. Distances d (Å) and polar angles θ and ϕ (deg) for Ti–O and K–O bonds in KTP, referred to the crystal (a, b, c) system. Errors are estimated to be one unit in the last digit.

$(Ti1)O_6$	d	θ	ϕ	$(Ti2)O_6$	d	θ	ϕ
O1	2.150	137.6	356.6	O3	2.044	98.2	347.0
O2	1.958	50.6	8.3	O4	1.981	86.8	173.0
O5	2.042	102.3	84.7	O7	1.965	48.3	270.5
O6	1.987	86.3	275.9	O8	1.990	141.7	86.3
OT1	1.981	140.1	190.1	OT1	1.733	48.9	73.7
OT2	1.716	47.2	167.9	OT2	2.092	134.6	258.4
$(K1)O_8$	d	θ	ϕ	$(K2)O_9$	d	θ	ϕ
O1	2.894	53.8	306.3	O1	2.677	109.3	127.3
O2	2.738	105.9	310.1	O2	2.982	49.3	131.0
O3	2.712	82.7	83.9	O3	3.045	1.4	182.1
O5	2.872	4.5	58.1	O4	3.117	126.3	266.5
O7	3.057	50.5	135.2	O5	2.806	84.5	181.3
O8	2.755	109.6	231.8	O7	2.918	102.9	50.1
OT1	2.996	53.6	236.8	O8	3.048	54.4	42.8
OT2	2.722	107.7	140.0	OT1	2.766	107.2	325.5
				OT2	3.057	52.3	335.4

planes perpendicular to the a and b axes, respectively, and one two-fold screw axis parallel to the c axis). Accordingly, the unit cell consists of eight formula $KTiOPO_4$. Distances and polar coordinates of the oxygen ligands for cation sites Ti1, Ti2, K1 and K2, are given in table 1.

As shown in figure 1 and table 1, potassium K1 is eight-fold coordinated by oxygen, K2 is nine-fold coordinated and Ti1 and Ti2 are six-fold coordinated. TiO_6 octahedra are linked by oxygens OT1 and OT2, whereas the remaining oxygen ligands belong to phosphate groups. It must be noted that the C_1 local symmetry of the TiO_6 octahedra can be approximated to tetragonal C_{4v} symmetry. This is because in each octahedron there is a shorter ($\approx$1.72 Å) 'titanyl' bond compared to the remaining Ti–O bonds (see table 1). The shortest-bond direction would indicate the approximate four-fold axis.

3. Results

The EPR spectrum of Er-doped KTP samples, measured at 5 K, is composed of various groups of lines. Each group consists of a strong peak, near the centre of the group, and a number of

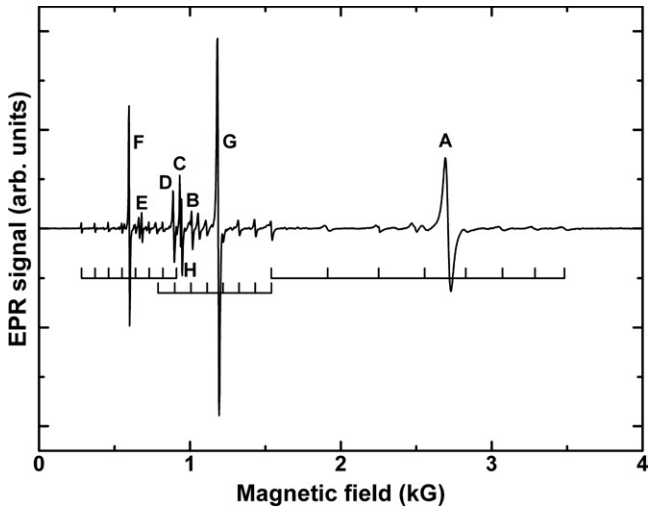

Figure 2. EPR spectrum of an Er-doped KTP sample measured at 5 K with the magnetic field $\boldsymbol{B}$ oriented along the b axis. Eight even-isotope lines have been labelled from A to H, corresponding to the eight Er^{3+} centres analysed in section 4. In the lower part, three eight-line patterns have been drawn for the hf structure of centres A, F and G, as calculated following the procedure explained in section 4.

satellite lines of much weaker intensity. The resonances appear in a wide magnetic field range from 400 G up to 13 000 G and have a typical peak-to-peak line-width around 10 G (at 5 K). All lines remain observable up to ∼18 K, which is a usual behaviour for rare-earth ions. For special orientations of the magnetic field $\boldsymbol{B}$ with respect to the crystallographic axes of KTP several groups collapse, giving rise to simpler spectra. The EPR spectrum for $\boldsymbol{B}$ parallel to the b axis is shown in figure 2. A detailed inspection of the spectra for $\boldsymbol{B}$ parallel to the crystallographic axes a, b and c reveals that they are composed of eight groups. The structure of each group (a strong peak and various satellite lines) is in agreement with the natural abundance ratio of the erbium isotopes. Thus the strong peaks would be related to the 77.1% abundant even isotopes with zero nuclear spin, while the satellite components would correspond to the hyperfine (hf) structure arising from the $I = 7/2$ nuclear spin of the ^{167}Er isotope, which is 22.9% abundant. According to this, the satellite lines show an eight-lines pattern corresponding to the normal 'allowed' transitions where the nuclear magnetic moment m does not change ($\Delta m = 0$), as marked in figure 2 for the three clearest groups. Therefore, we attribute the whole observed spectrum to different erbium centres. More specifically, we attribute it to eight trivalent erbium centres, as shown below. These centres have been labelled from A to H.

The Er^{3+} ion has a $4f^{11}$ configuration and a $^4I_{15/2}$ free-ion ground level. Group Theory considerations show that this ground level splits into eight Kramers doublets for crystal fields whose symmetry is lower than cubic. This splitting is, generally, large enough so that only the lowest lying doublet is appreciably populated at low temperatures. So, EPR signals would be observed only for this doublet, which can be described in an effective $S' = 1/2$ notation. This means that each group of lines should be attributed to a particular orientation of an Er^{3+} related centre.

The angular dependence of the EPR spectra has been studied with the magnetic field $\boldsymbol{B}$ varying in the three crystallographic planes, i.e. planes ab, bc and ca (see figure 3). For simplicity only the intense even-isotope lines have been plotted as open circles. When the magnetic field deviates in each plane from the a, b or c axes, each line splits into two. Moreover,

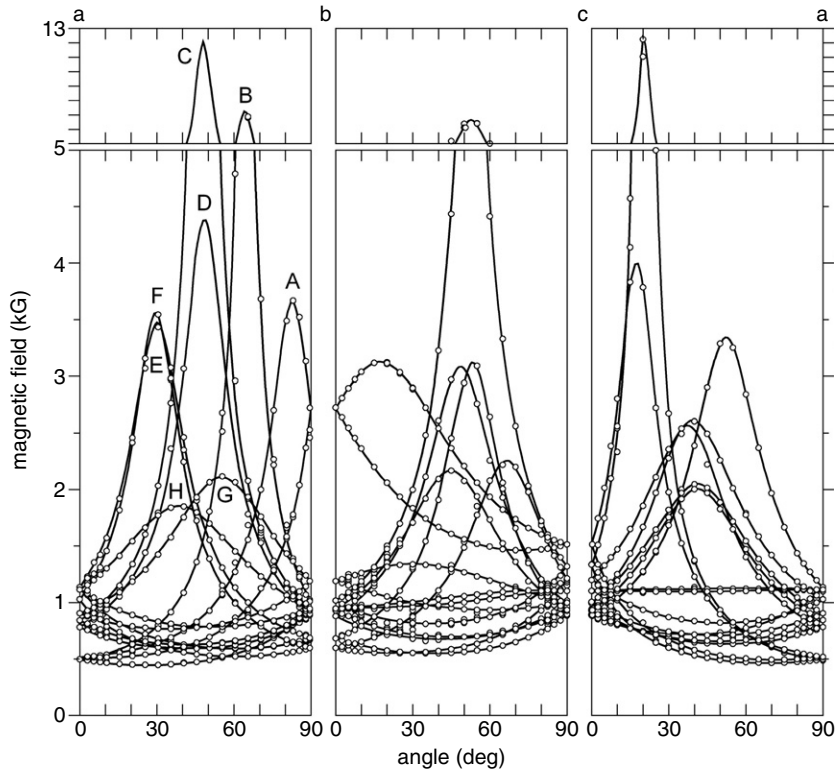

Figure 3. Angular dependence of the EPR spectrum of centres A to H in crystal planes *ab*, *bc* and *ca* of KTP. Experimental resonance-field positions of even-isotope lines are plotted with open circles. Calculated angular dependences are plotted with continuous lines.

if the magnetic field is tilted out of the plane the lines split again into two, giving a maximum of 32 even-isotope lines. This behaviour agrees with the symmetry properties of the KTP lattice given above.

4. Analysis and discussion

To analyse the EPR spectra and their angular dependences, the appropriate spin-Hamiltonian for an effective spin $S' = 1/2$ and nuclear spin $I = 7/2$ is [17]

$$\hat{H} = \mu_B \vec{B} \hat{\hat{g}} \hat{\vec{S}}' + \hat{\vec{S}}' \hat{\hat{A}} \hat{\vec{I}} - g_n \mu_n \vec{B} \hat{\vec{I}}, \tag{1}$$

where the three terms represent the electronic Zeeman interaction, the hyperfine interaction and the nuclear Zeeman interaction, respectively. The last term has been neglected since it is small and gives corrections to the EPR lines positions below experimental error. It must be noted that only the intense even-isotope lines can be followed along the whole range of study of the angular dependences, so the hyperfine structure cannot be analysed. Despite this, we have employed the first two terms of equation (1) to calculate the three hf groups of the eight-line patterns shown in figure 2. We have employed the $\boldsymbol{g}$-matrices for centres A, F and G resulting from the analysis and fitting procedure given below, taking $\boldsymbol{B}$ parallel to the b axis. The corresponding $\boldsymbol{A}$-matrices have been constructed assuming they have the same principal axes as the $\boldsymbol{g}$-matrices. The principal A-values of each centre have been estimated from the

Table 2. Diagonal form of fitted $\boldsymbol{g}$-matrices for Er^{3+} centres A–H observed in KTP at 5 K, referred to the crystal (a, b, c) system. Errors are shown in brackets for the last digit. For a better comparison between the directions of X, Y and Z for the different centres, all axes shown have $\theta < 90°$ by changing the sign of direction cosines of those axes initially with $\theta > 90°$.

			Principal directions	
Centre	Principal values	Mean g-value	θ	ϕ
	$g_X = 1.104(2)$		44.9(1)	115.5(1)
A	$g_Y = 2.275(1)$	5.738(2)	50.3(1)	262.0(1)
	$g_Z = 13.835(2)$		72.6(1)	7.1(1)
	$g_X = 0.31(4)$		38(1)	141(1)
B	$g_Y = 1.09(2)$	5.81(3)	59(1)	283.8(6)
	$g_Z = 16.01(3)$		71.6(1)	25.6(1)
	$g_X = 3.678(1)$		31.6(1)	219.0(1)
C	$g_Y = 0.550(1)$	5.551(1)	88.7(1)	311.1(1)
	$g_Z = 12.425(1)$		58.4(1)	42.0(1)
	$g_X = 2.66(2)$		32.1(5)	196(2)
D	$g_Y = 1.45(5)$	5.72(4)	78(1)	305.0(7)
	$g_Z = 13.04(5)$		60.5(2)	41.7(2)
	$g_X = 1.935(1)$		81.0(2)	155.7(2)
E	$g_Y = 2.166(1)$	5.869(1)	34.4(1)	259.0(4)
	$g_Z = 13.507(1)$		57.2(1)	59.8(1)
	$g_X = 1.866(8)$		82.6(4)	153.0(2)
F	$g_Y = 2.996(7)$	6.206(8)	22.0(1)	262(1)
	$g_Z = 13.756(9)$		69.4(1)	60.2(1)
	$g_X = 1.674(1)$		61.0(1)	141.5(1)
G	$g_Y = 5.109(1)$	5.668(1)	47.9(1)	261.6(1)
	$g_Z = 10.221(1)$		55.8(1)	29.4(1)
	$g_X = 6.118(5)$		4.1(2)	203(2)
H	$g_Y = 3.631(9)$	6.118(8)	88.0(2)	321.4(6)
	$g_Z = 8.604(9)$		86.4(2)	51.5(6)

following relationships: $A_X/g_X = A_Y/g_Y = A_Z/g_Z = A_J/g_J$, where $A_J = -125$ MHz is the magnetic hyperfine constant of the ^{167}Er isotope for the $^4I_{15/2}$ free-ion ground level of Er^{3+} and $g_J = 1.2$ is the Landé g-factor [17]. In spite of these assumptions, the simulated hyperfine patterns allow us to explain satisfactorily the hf components of these three centres, as can be observed in figure 2. This confirms that these centres correspond to Er^{3+} ions.

On the other hand, to determine the $\boldsymbol{g}$-matrices for the eight centres only the electronic Zeeman interaction is left in the Hamiltonian of equation (1). A computer program has been used to diagonalize the corresponding energy matrix for a number of magnetic field orientations. The program also performs a least-squares fitting procedure to the experimental even-isotope line positions. In the current study, an average of 115 independent line positions was used for each centre as input data, along with the corresponding microwave frequencies. The resulting best-fit matrices are shown in diagonal form in table 2. Note that we are assuming symmetric $\boldsymbol{g}$-matrices, with only six independent elements (g_{aa}, g_{bb}, g_{cc}, $g_{ab} = g_{ba}$, $g_{ac} = g_{ca}$ and $g_{bc} = g_{cb}$ referred to the crystal (a, b, c) system). This is because the standard EPR measurements in low-symmetry systems are not able to detect asymmetries [18]. Errors in the principal g-values and directions shown in table 2 are obtained from the least-squares procedure used by considering a 6 G uncertainty in the measured line position. Subsequently, the matrices

were used to calculate the solid lines depicted in figure 3. As observed, the agreement between experiment and theory is very good.

Some comments need to be made about the various best-fit matrices (g_{aa}, g_{bb}, g_{cc}, g_{ab}, g_{ac}, g_{bc}) that can be obtained using the experimental line position in the crystal planes ab, bc and ac. We have obtained eight different best-fits for each centre, each fit giving an identical minimum value of the least-squares function. The eight best-fit matrices are divided into two groups of four, each matrix in one group having equal absolute values of the matrix elements but with opposite sign with respect to one matrix in the other group (equal absolute value of the matrix trace but positive or negative). The four matrices of one group have different values of the elements. After diagonalization, the four matrices with the same trace sign have the same principal g_Z-value and equal absolute values of g_X and g_Y, but differ in the four possible combinations of signs for g_X and g_Y. The principal Z axes are identical, whereas X and Y appear for some matrices with different orientation, but always with the same directions, i.e., if one X or Y axis has direction cosines $[l, m, n]$, for the other matrix these can appear as $[-l, -m, -n]$. Finally, for the second group with the other trace sign diagonalization gives the same absolute values as for the first group, but with a sign change of all principal values and direction cosines. These results are related to the fact that the absolute and relative signs of the principal g-values cannot be determined by usual EPR spectroscopy [17–19], i.e., using linearly polarized microwave radiation and line positions as experimental data only. In fact, we have measured a fourth angular dependence with the magnetic field lying in a skew plane to try to disclose which of the eight best-fit matrices for each centre could be the correct one. The result is that all eight best-fit matrices of each erbium centre give the same calculated line positions for this angular dependence, which, on the other hand, agree very well with the experimental ones. Therefore, since at the present time we cannot carry out experiments and calculations to determine the correct combination of signs for each centre, table 2 shows the fit with positive values, as is usually done in many works found in the literature [17].

On the other hand, it must also be noted that each best-fit matrix for each centre represents four matrices, which are related to the four equivalent orientations of the corresponding centre in the KTP lattice (see section 2). For the diagonal form of the matrices, this means that if the orientation of one principal axis for one centre is described by the direction cosines $[l, m, n]$, the three other orientations of this axis are $[-l, m, n]$, $[l, -m, n]$ and $[-l, -m, n]$. For further discussion below, note that in terms of polar angles θ and ϕ the four orientations have the same θ-value and different ϕ-values.

The assignment of the observed EPR spectra to defects associated to Er^{3+} is supported by the previous explanation of the hyperfine structure in the spectrum, the effective spin $S' = 1/2$ used to fit the spectra and the experimental mean g-value $\bar{g} = (g_X + g_Y + g_Z)/3$. These mean values range from 5.55 to 6.21 for the eight centres (table 2), which are typical values for Er^{3+} in several hosts, where g_X, g_Y and g_Z are also assumed positive, with values ranging from 5.1 to 6.8 [17, 19].

With regard to the location of Er^{3+} ions, there are four cation sites where erbium can enter, two Ti^{4+} sites and two K^+ sites, as described in sections 1 and 2. The various transition elements already studied in KTP by EPR [3–10] have always been found substituting for both Ti^{4+} sites, except for Pt^+ [10]. Also, as explained in section 1, RE ions Nd^{3+} and Er^{3+} [11, 12] have been assumed to be located at Ti^{4+} sites. However, it must be remarked that in these works substitution for Ti by Er^{3+} or Nd^{3+} was considered based on the results from crystal growth experiments only. The fact that the distribution coefficients of different RE ions in KTP crystals decreases as their ionic radius increases [14] suggested that trivalent RE ions substitute the Ti^{4+} of the lattice. The only structural study developed by x-ray single-crystal diffraction on Nd-doped KTP crystals grown on a solution containing W did not take into account neodymium

in the refinement of the structure, due to the low doping level [20]. Another argument used to assign the position of Nd^{3+} in KTP crystals was the comparison of the spectral position of one of its electronic levels with respect to other lattices [11, 21]. However, in those works the authors pointed out that substitution for K by Nd and other RE ions could not be fully excluded on the basis of the spectroscopic results. Potassium sites in the KTP structure have the same low symmetry as titanium ones and would induce a similar lifting of the multiplet degeneracy. More recent structural studies on $RbTiOPO_4$ crystals codoped with Nb and Er [22, 23] concluded that Er occupies Ti positions. However, the concentration of Er in these crystals is three orders of magnitude higher than in the KTP crystals studied here. Furthermore, the Nb concentration in those crystals is four times larger than the concentration of Er, whereas our KTP crystals do not contain any codopant. Therefore, we think that these results are not applicable to our case.

In this work, we use the resulting matrices in table 2 to propose the location of Er^{3+} in KTP. First, it must be noted that the principal values for most centres shown in table 2 indicate a strong axial character, the Z-axis being assigned to the largest principal g-value. One could expect the principal axis Z to be close to the direction of some of the cation–oxygen bonds, as found for various axial centres of transition elements with $S' = 1/2$ studied by EPR in KTP [5–10]. In such axial cases, the axis Z was found nearly along the shortest 'titanyl' bonds (see section 2), which enabled the assignment to the Ti sites. For the present case of Er, one can compare each Z-axis for the eight centres in table 2 to Ti–O and K–O bond directions shown in table 1. For both Ti sites, the Z-axis is not close to any of the shortest 'titanyl' bond directions for the eight centres. In principle, this result would exclude substitution for Ti, although one has to bear in mind that upon Er doping the cation–oxygen distances may change significantly, as well as the expected principal directions, due to possible charge-compensating defects in the close vicinity of Er. On the other hand, the K–O bond directions for both K1 and K2 sites can be grouped into two families whose polar angles θ are near 52° and 107°, respectively (see table 1). Despite the C_1 local symmetry of the K sites, these angles compare well to the θ-values of axes Z which are near 58° and 110° (180°–70°) except for the less axial centre (centre H) which is 86° (see table 2). Such positive comparisons strongly point to Er^{3+} being located at K^+ sites for the eight centres A to H. This proposal would indicate that Er^{3+} ions with larger ionic radius (0.96 Å) than those for transition elements cannot be accommodated in the Ti^{4+} site (0.68 Å).

Finally, as there are two K^+ sites in the lattice and eight different centres one has to consider some perturbation making the difference. It is reasonable to think that the compensation of the charge misfit between Er^{3+} and K^+ could be reached through K^+ vacancies close to Er^{3+} ions, giving rise to the different observed centres.

In short, our EPR results show the formation of eight Er^{3+} centres in KTP single-doped with erbium at a low concentration level. Although substitution for Ti cannot be fully excluded, the fitted g-matrices strongly point to Er^{3+} ions being located at both K^+ sites for the eight centres. The appearance of such a large amount of centres would be related to charge-compensating defects in the close vicinity of Er^{3+}, probably K^+ vacancies.

Acknowledgments

This work has been supported by DGESIC and CICyT under projects BFM2001-0221, MAT2002-04603, CIT-020400-2005-14 and MAT2005-06354-C03-02.

References

[1] Zumsteg F C, Bierlein J D and Gier T E 1976 *J. Appl. Phys.* **47** 4980–5
[2] Bierlein J D and Vanherzeele H 1989 *J. Opt. Soc. Am.* B **6** 622–33

[3] Gaite J M, Stenger J F, Dusausoy Y, Marnier G and Rager H 1991 *J. Phys.: Condens. Matter* **3** 7877–86
[4] Ahn S W and Choh S H 1999 *J. Phys.: Condens. Matter* **11** 3193–9
[5] Vassilikou-Dova A B, Jansen S, Wallrafen F and Lehmann G 1989 *Z. Naturf.* A **44** 711–4
[6] Han S, Wang J, Xu Y, Liu Y and Wey J 1992 *J. Phys.: Condens. Matter* **4** 6009–14
[7] Geifman I N, Usov A N and Nagornyi P G 1992 *Phys. Status Solidi* b **172** K73–6
[8] Bravo D, Martín M J, Gavaldá J, Díaz F, Zaldo C and López F J 1994 *Phys. Rev.* B **50** 16224–31
[9] Bravo D, Ruiz X, Díaz F and López F J 1995 *Phys. Rev.* B **52** 3159–69 and references therein
[10] Garces N Y, Stevens K T and Halliburton L E 2000 *J. Appl. Phys.* **87** 8682–7
[11] Zaldo C, Aguiló M, Díaz F and Loro H 1996 *J. Phys.: Condens. Matter* **8** 10693–701
[12] Rico M, Zaldo C, Massons J and Díaz F 1998 *J. Phys.: Condens. Matter* **10** 10101–13
[13] Kling A, Rico M, Zaldo C, Aguiló M and Díaz F 2004 *Nucl. Instrum. Methods Phys. Res.* B **218** 271–6
[14] Solé R, Nikolov V, Koseva I, Peshev P, Ruiz X, Zaldo C, Martín M J, Aguiló M and Díaz F 1997 *Chem. Mater.* **9** 2745–9
[15] Tordjman I, Masse R and Guitel J C 1974 *Z. Kristallogr.* **139** 103–15
[16] Thomas P A, Glazer A M and Watts B E 1990 *Acta Crystallogr.* B **46** 333–43
[17] Abragam A and Bleaney B 1970 *Electron Paramagnetic Resonance of Transition Ions* (New York: Clarendon/Oxford University Press)
[18] Pilbrow J R and Lowrey M R 1980 *Rep. Prog. Phys.* **43** 433–95
[19] Ammerlaan C A J and de Maat-Gersdorf I 2001 *Appl. Magn. Reson.* **21** 13–33
[20] Solé R, Ruiz X, Cabré R, Gavaldá J, Aguiló M, Díaz F, Nikolov V and Solans X 1996 *J. Cryst. Growth* **167** 681–5
[21] Zaldo C, Martín M J, Solé R, Aguiló M, Díaz F, Roura P and López de Miguel M 1998 *Opt. Mater.* **10** 29–37
[22] Carvajal J J, García-Muñoz J L, Solé R, Gavaldá J, Massons J, Solans X, Díaz F and Aguiló M 2003 *Chem. Mater.* **15** 2338–45
[23] Carvajal J J, García-Muñoz J L, Solé R, Gavaldá J, Massons J, Aguiló M and Díaz F 2003 *J. Solid State Chem.* **171** 257–61